ADVANCED FUNCTIONAL MATERIALS
www.afm-journal.de

Self-Assembled Complexes of Horseradish Peroxidase with Magnetic Nanoparticles Showing Enhanced Peroxidase Activity

Stéphane C. Corgié, Patarawan Kahawong, Xiaonan Duan, Daniel Bowser, Joseph B. Edward, Larry P. Walker, and Emmanuel P. Giannelis*

Bio-nanocatalysts (BNCs) consisting of horseradish peroxidase (HRP) self-assembled with magnetic nanoparticles (MNPs) enhance enzymatic activity due to the faster turnover and lower inhibition of the enzyme. The size and magnetization of the MNPs affect the formation of the BNCs, and ultimately control the activity of the bound enzymes. Smaller MNPs form small clusters with a low affinity for the HRP. While the turnover for the bound fraction is drastically increased, there is no difference in the H_2O_2 inhibitory concentration. Larger MNPs with a higher magnetization aggregate in larger clusters and have a higher affinity for the enzyme and a lower substrate inhibition. All of the BNCs are more active than the free enzyme or the MNPs (BNCs > HRP >> MNPs). Since the BNCs show surprising resilience in various reaction conditions, they may pave the way towards new hybrid biocatalysts with increased activities and unique catalytic properties for magnetosensitive enzymatic reactions.

1. Introduction

Magnetic fields have long been suspected of influencing biological reactions involving free-radicals.[1–6] However, strong magnetic fields are rare in the biological world and evidence of low-magnetic-field effects is yet to be demonstrated unequivocally.[7–9] More recently, the effect of high magnetic fields has been shown on various free-radical-producing enzymes.[6,10] The relationship between magnetic fields and enzymatic activity has mostly been explained in the context of radical recombination and the intersystem-crossing (ISC) mechanism:[11,12] localized and medium-to-strong magnetic fields can significantly affect the extent of radical-pair recombination under specific ranges of intensity and reaction conditions. The relative reorientation of two spins resulting from ISC in chemical reactions involving superparamagnetic species can be theoretically accomplished with moderate-to-strong magnetic fields such as those generated by magnetic nanoparticles (MNPs).[13] Randomly distributed MNPs could therefore play a significant role in chemical and biochemical reactions involving spin-correlated radical pairs[14–16] as each individual nanoparticle generates its own localized and intense magnetic field.

Peroxidase-like activity has been reported in large magnetite nanoparticles void of any enzyme. This activity has been shown to follow Michaelis–Menten kinetics and to be sensitive to H_2O_2 and pH.[17,18] However, our own studies have shown that enzymatic peroxidase activities were always several orders of magnitude higher in comparison with MNP peroxidase-like activities, in the range of the hydrogen peroxide concentrations used.[19] Horseradish peroxidase (HRP) has been widely studied because of its relevance and its potential applications in biomedical, environmental and industrial biotechnologies.[20,21] Peroxidases (EC 1.11.1) are widely found in biological systems and form a subset of oxidoreductases that reduce hydrogen peroxide (H_2O_2) to water in order to oxidize a large variety of aromatic compounds ranging from phenol to aromatic amines. The reaction cycle of peroxidases is quite complex and begins with activation of the heme by H_2O_2 to form the two-electron activated Compound I.[21] Compound I is then reduced by one electron by the oxidation of the organic substrate, leading to the formation of Compound II, which is one electron above the resting state. The second reduction brings back the enzyme to its resting state to start a new cycle. Overall, for each molecule of hydrogen peroxide consumed, two aromatic free-radicals are produced and they can react readily in secondary reactions. Peroxidases, in general, are highly sensitive to substrate inhibition,[22–26] mostly by H_2O_2, which can lead to the formation of the reversible, inactivated form of the enzyme (Compound

Dr. S. C. Corgié
Biofuels Research Laboratory
Cornell University
Ithaca, NY 14853, USA
E-mail: scc37@cornell.edu
Dr. S. C. Corgié, D. Bowser, J. B. Edwards, Prof. L. P. Walker
Biological and Environmental Engineering
Cornell University
Ithaca, NY 14853, USA
P. Kahawong, X. Duan, Prof. E. P. Giannelis
Department of Materials Science and Engineering
326 Bard Hall, Cornell University
Ithaca, NY 14853, USA

DOI: 10.1002/adfm.201102398

III). Therefore, peroxidase-enzyme kinetics are quite complex and their activities are highly sensitive to the initial reaction conditions, which restricts their use in many bioprocesses. Increasing the activities of this family of enzymes and their tolerance to different process conditions might pave the way for new applications, especially when controlling and improving the efficiency of free-radical-mediated reactions is involved.

As reported by Tabaran et al.,[27] the HRP reaction cycle involves the sequential formation of several paramagnetic species, and theoretical models have been developed to predict either beneficial or detrimental effects of the magnetic-flux intensity.[4,27] However, the influence of external magnetic fields on the reaction rates and mechanisms involving peroxidase enzyme is still controversial.[28] Here, we investigate the peroxidase activities of two magnetite nanoparticles, referred to as M25 and M90, in combination with HRP. In addition, we elucidate the kinetics of these magnetic enzyme-MNPs self-assembled complexes. This simple approach, focusing on the tightly bound fraction of the enzyme, differs sharply from classical methods requiring protein conjugation onto surface-modified particles by complex biochemistries, often at the expense of enzymatic activities and reaction efficiencies. We demonstrate that HRP kinetics are modified profoundly only when the enzymes are in close association with the MNPs and that the overall activities of the bio-nanocatalysts (BNCs) are then orders of magnitude higher than those of free enzymes or MNPs at biologically relevant substrate concentrations. The insights gained regarding MNP-HRP complex formation and activity open new opportunities to expand the use, scale and efficiency of free-radical-mediated reactions thanks to nanoscale and self-assembled hybrid catalysts relying on: 1) the clustering properties of the MNPs, 2) magnetic-field effects at the nanoscale, and 3) the resulting enzyme kinetics, which are sensitive to magnetic fields.

2. Results

2.1. Magnetite MNP Characteristics

MNPs are easy to mass produce. The synthesis requires low-cost reagents and can be easily tailored for size, magnetic field and surface properties.[29] The average calculated particle sizes for M25 and M90 were 8 and 10 nm, respectively. The particle-size values were obtained from transmission electron microscopy (TEM) images (**Figure 1**A,B) and were in good agreement with the average diameter calculated from the Scherrer equation (Table S1, Supporting Information). M90 had a more uniform size distribution, with an average size of 10 ± 1 nm (Figure 1D) while M25 had a broader size range with an average size of 8 ± 3 nm, with particles as small as 5 nm (Figure 1C). The physical and magnetic properties of the MNPs are presented in Table S1, Supporting Information. Both types of MNP had, overall, negligible remanent magnetization (M_R) indicating superparamagnetism (Figure 1E). At the concentration of magnetite used for the assays, the M25 MNPs were mostly monodisperse with small clusters and free nanoparticles (**Figure 2**), whereas M90 formed large clusters with a diameter of 100 nm, on average (**Figure 3**). The total pore volumes were 0.39 $cm^3\ g^{-1}$ and 0.14 $cm^3\ g^{-1}$ for M90 and M25, respectively. The average densities of the clusters, when corrected for the porosity, were ρ_{M25} = 3.03 g cm^{-3} and ρ_{M90} = 1.72 g cm^{-3}.

2.2. BNCs: HRP and MNP Self-Assembly

M90 had a higher value of K_a than M25, indicating a higher affinity for the HRP enzyme (Figure 1F). From Equation 1, it was found that less than 50% of the total HRP loaded could bind to M25 to form the M25-BNC complex when 1×10^{-9} M HRP and 4 μg mL^{-1} magnetite particles were used, while all of the enzyme was adsorbed in the case of M90 (**Table 1**). The point of zero charge (PZC) of the magnetite was found to be at around pH = 7.9, while the isoelectric point of HRP is at around pH = 7.2. For this study, the BNCs were formed in ultrapure water at pH = 6.5, implying the presence of $Fe–OH^{2+}$ cationic species on the nanoparticle surfaces. At this pH and in the absence of any other compensating charges, a large surface of the HRP molecules remains negatively charged[30] allowing the formation of complexes with magnetite via electrostatic interactions.[31] Given the fact that M25 and M90 have the same surface composition and that their surface areas differ by about 20%, the 9.1% difference in the maximum binding capacity (Q_m) between the M25- and M90-BNCs cannot be attributed only to a surface effect.

Both the types of MNP clustered and formed aggregates due to the magnetization that each particle could experience when in close vicinity to each other. Nanosized particles usually generate high magnetic-field gradients. The M90-cluster density was about 33% lower than that of M25 clusters, due to its pore structure. This explains why, even if single M25 nanoparticles induce lower magnetic fields than the bigger M90 ones because of their lower mass magnetization, the M25 clusters had a higher field, as the aggregate density plays a significant effect (Figure S1, Supporting Information). The M90-MNPs formed bigger and denser aggregates (Figure 3) not only because of the higher magnetic attraction, but also to reduce the energy associated with their high surface-area-to-volume ratio. Adsorbed enzyme molecules onto the MNPs could then be further entrapped within these clusters,[32] as observed by the increase in the size of the BNC clusters (Figure 2 and 3) and the difference in the HRP-adsorption behaviors of M25 and M90 (Figure S2, Supporting Information). Both the BNCs were mesoporous. The M90-BNCs had a higher total pore volume and a higher average pore size than the M25-BNCs. The differences in the formation of the complexes were consequently attributed to the ultrastructure of the MNPs clusters resulting from differences in the magnetization of the nanoparticles and the resulting mesoporosity of the clusters. M90-BNC self-assembly would therefore result from a dual mechanism of surface adsorption and molecular entrapment in the mesoporous aggregates (Figure 3D, Figure S2, Supporting Information).

2.3. The Magnetic Field Effect Acts Only on the Bound Fraction of the Enzymes

Temporal free-radical concentrations were measured using the phenol/4-aminoantipyrine (AAP)[19] assay in malonate buffer,

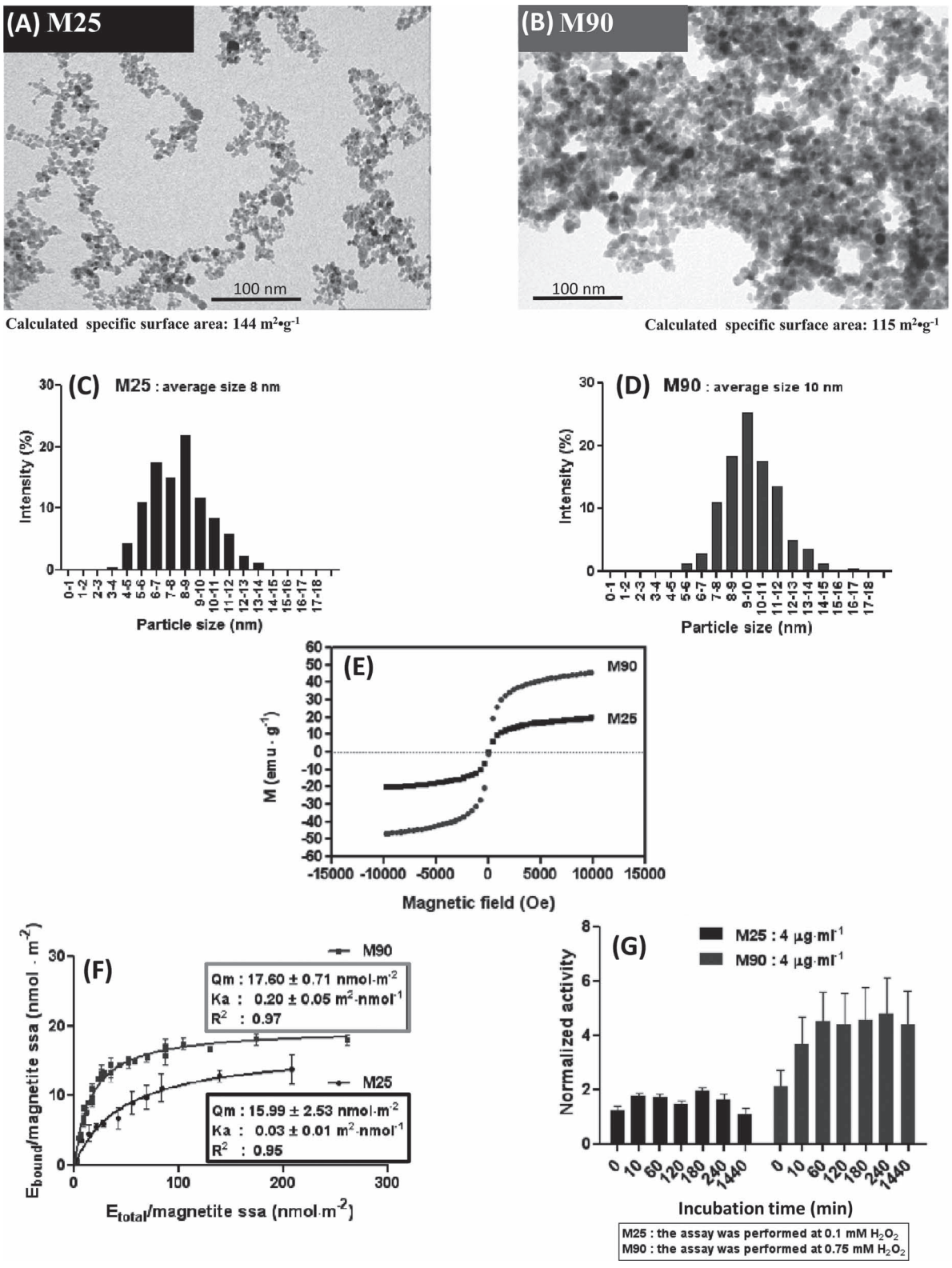

Figure 1. A–G) MNP and BNC characterization: TEM pictures of M25 and M90 magnetite nanoparticles (A–B); particle-size distribution (C–D); magnetization hysteresis curves (E); HRP adsorption isotherms onto M25 and M90 in water, with estimated K_a and Q_m (F); normalized activity of M25-BNCs (1×10^{-9} M, 46% bound, 5% Q_m) and M90-BNCs (1×10^{-9} M, 100% bound, 30.3% Q_m) at their respective H_2O_2 optimal concentration as a function of BNC incubation time (pH = 3, 2.9×10^{-3} M malonate buffer, 25 °C) (G).

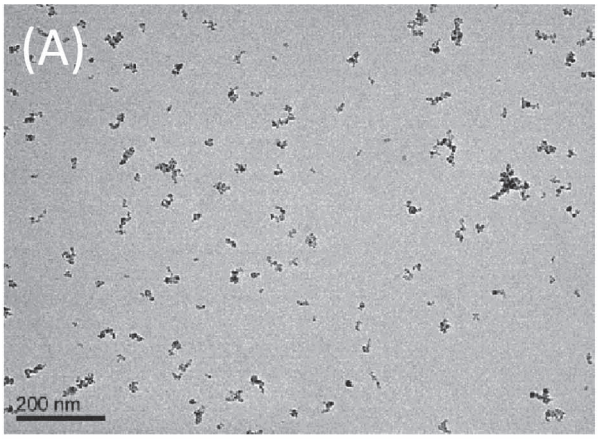

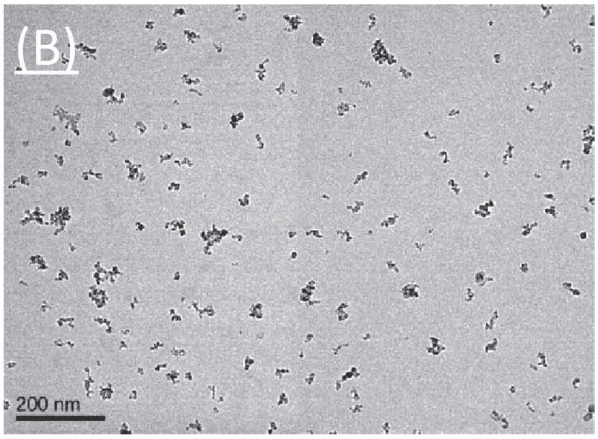

M25

Average perimeter: 56.6 nm
Average area:74.5 nm^2
Average Equivalent Circular Diameter: 8.5 nm

M25-BNCs

Average perimeter: 67.9 nm
Average area:123.3 nm^2
Equivalent Circular Diameter: 11.6 nm

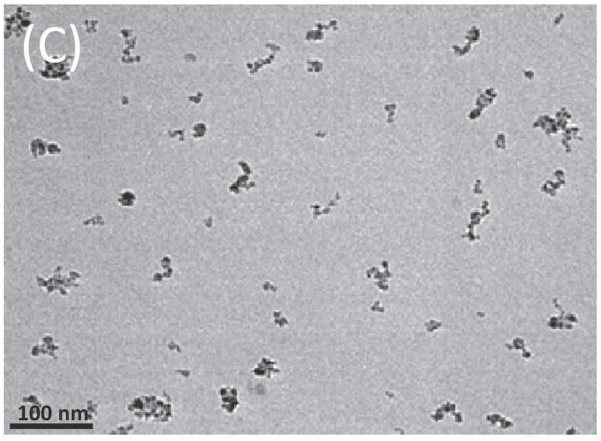

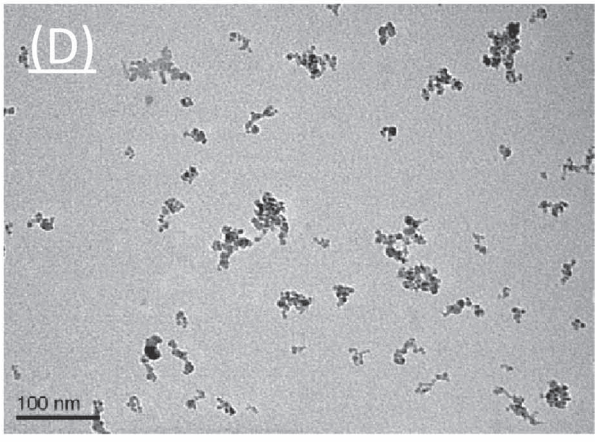

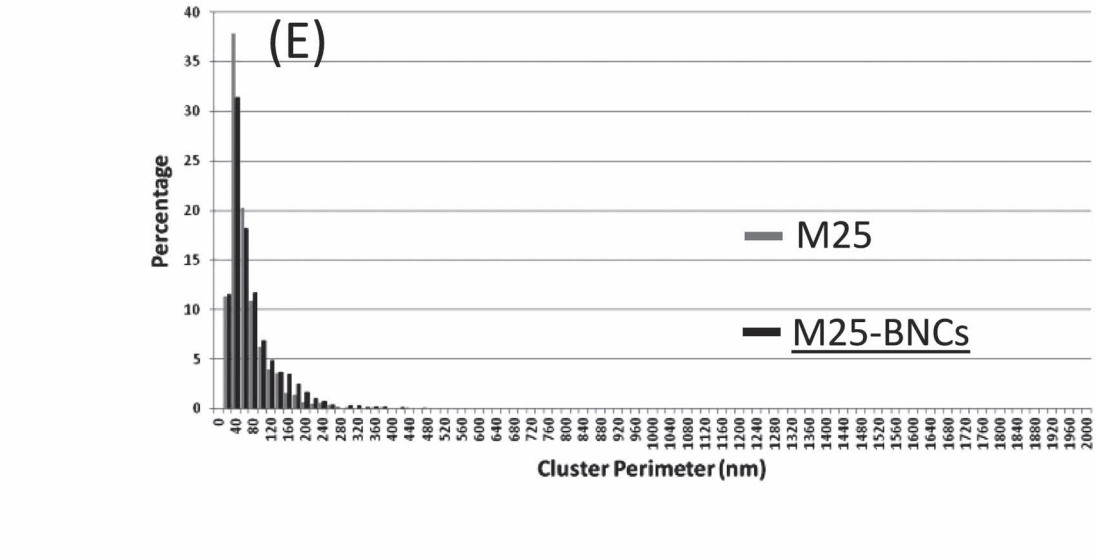

Figure 2. A–D) Representative TEM images of M25-MNPs (A–B) and M25-BNCs clusters (C–D) (1×10^{-9}M HRP) at 4 μg mL^{-1} of MNPs. E) Size distributions of M25 and M25-BNCs (perimeter of the clusters, 2500 clusters).

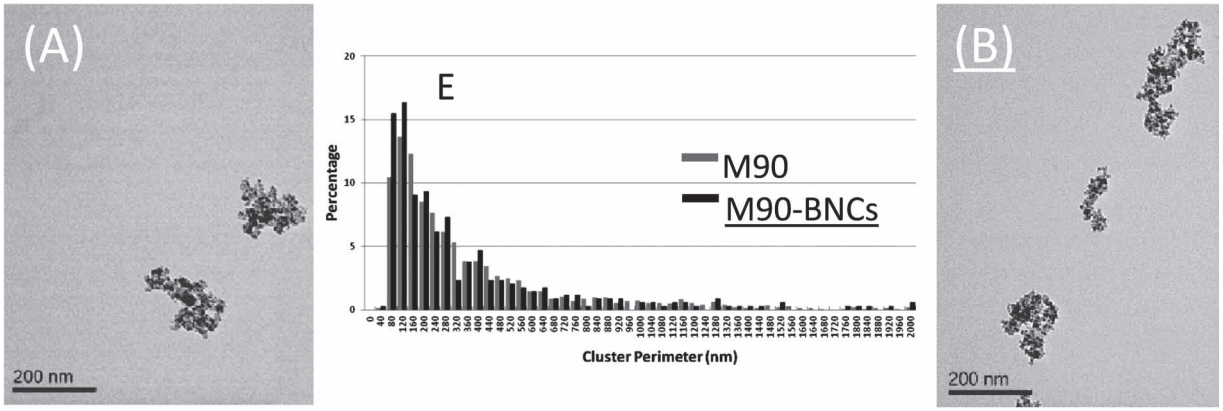

M90
Average perimeter: 425 nm
Average area: 6752 nm^2
Average Equivalent Circular Diameter: 63.9 nm

M90-BNCs
Average perimeter: 652 nm
Average area: 18580 nm^2
Average Equivalent Circular Diameter: 102.3 nm

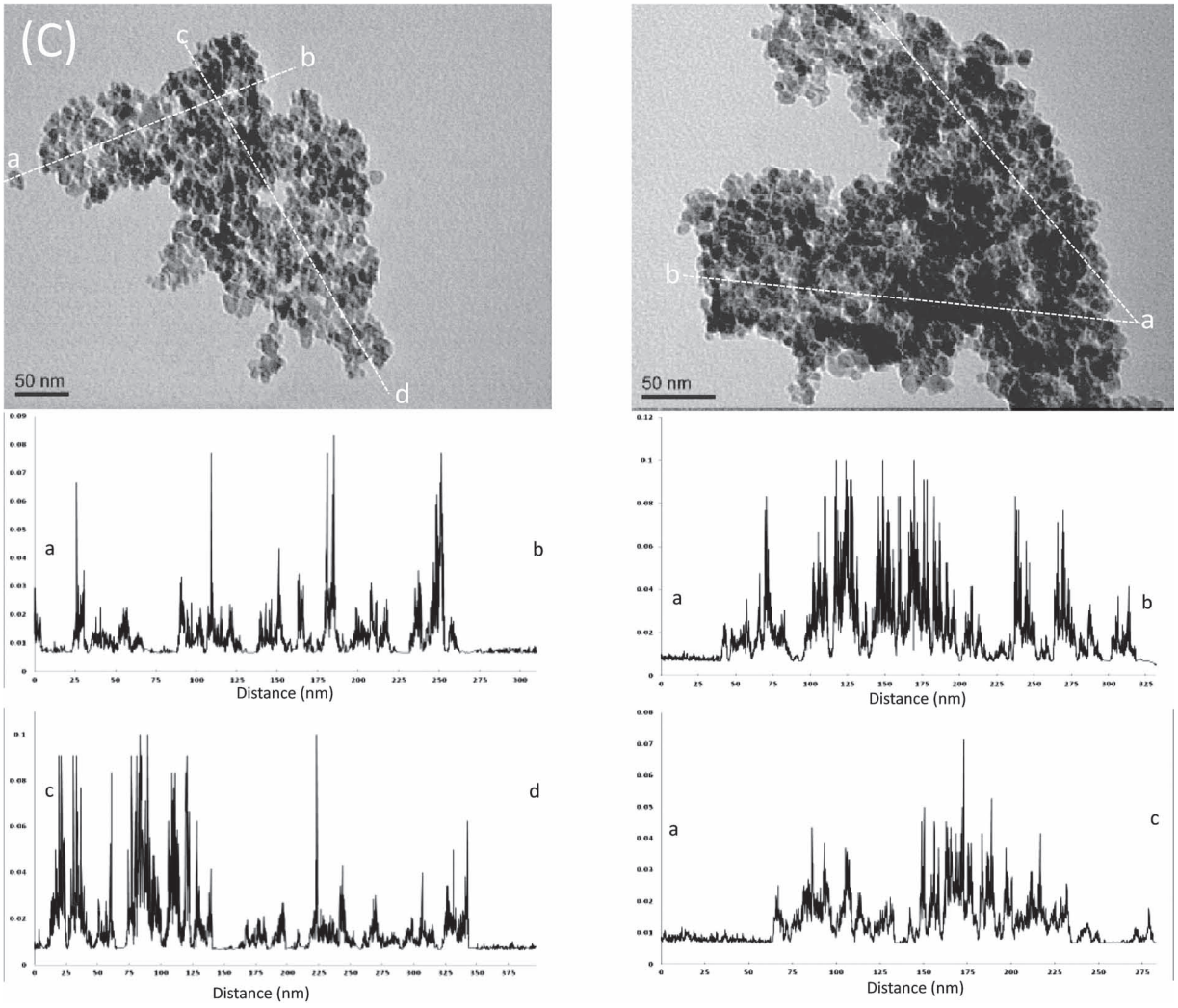

Figure 3. A–D) Representative TEM images of M90-MNPs (A–B) and M90-BNC clusters (C–D) (1×10^{-9} M HRP) at 4 μg mL^{-1} of MNPs. Transects (background-corrected pixel intensity) are presented for the higher magnification TEM images for M90 (C) and the M90-BNCs (D). E) Size distributions of M90 and M90-BNCs (perimeter of the clusters, 1000 clusters from TEM images of 40 μg mL^{-1} of MNPs).

Table 1. The percentage of bound HRP (from initial concentrations of 0.5×10^{-9}, 1×10^{-9} and 2×10^{-9} M), the quantity of HRP per MNP surface area, the percentage of surface saturation and the maximal normalized activity for M25-BNCs and M90-BNCs at 4 μg MNP mL^{-1} and at 0.75×10^{-3} and 2.5×10^{-3} M H_2O_2 respectively.

Concentration of bound HRP [$\times 10^{-9}$ M]	Percentage of bound enzyme [%]	Amount of bound enzyme [nmol m^{-2}]	Percentage of surface saturation [%]	Maximal normalized activity
M25-BNC 0.23	43.75	0.4	2.54	2.5 ± 0.5
M25-BNC 0.46	45.6	0.79	4.95	3.6 ± 0.1
M25-BNC 0.9	46.75	1.5	9.43	2.2 ± 0.1
M90-BNC 0.5	100	2.2	17.86	6.9 ± 0.6
M90-BNC 1	100	4.3	30.3	13.2 ± 0.8
M90-BNC 2	100	8.7	46.51	14.1 ± 1.3

and these measurements were used to calculate the normalized activities of the BNCs (Figure 1G). The normalized activities were calculated as the ratio of the BNC activity and the free-enzyme activity at the same concentration. For the M90-BNC, the maximum activity, compared with that of the free enzyme, was reached after 1 h of preincubation. The increase of the normalized activity was shown to be stable over 24 h. The M25-BNC reached maximum increased activity after incubation for 10 min. A zero, or limited, increase in the rate of the reaction was observed when the nanoparticles, enzyme and substrates were added simultaneously, regardless of the buffer, nanoparticles, substrates or enzyme concentration (data not shown).

These results clearly demonstrate that the increased activity was only due to the immobilized enzyme and not just the presence of the MNPs in solution. This constitutes the first experimental evidence of a need for a close association between enzymes and MNPs as a requirement to increase enzymatic activity. Moreover, the results also demonstrate that the association of HRP with magnetite nanoparticles of different sizes and magnetism yields different complexes with different specific activities. The importance of complex formation on the peroxidase reaction velocities becomes evident when comparing the velocities of bound enzymes (**Figure 4**) with the activities of the M25- and M90-BNCs at different HRP-to-MNP ratios (Figure S3, Supporting Information). The reaction velocities were comparable for all of the M90-BNCs, while the activities of the M25-BNCs were correlated with the enzyme-to-MNP ratio. The difference in activity response to the enzyme-to-MNP ratios between the BNCs can be attributed to the complete binding of the loaded enzymes for the M90-BNCs, and a partial binding in the case of the M25-BNCs. These results also confirmed the Fourier transform IR (FTIR)-spectroscopy measurements, indicating that all the enzyme molecules were associated with the M90-MNPs. For both the BNCs, the concentration of the MNPs did not matter in terms of the overall

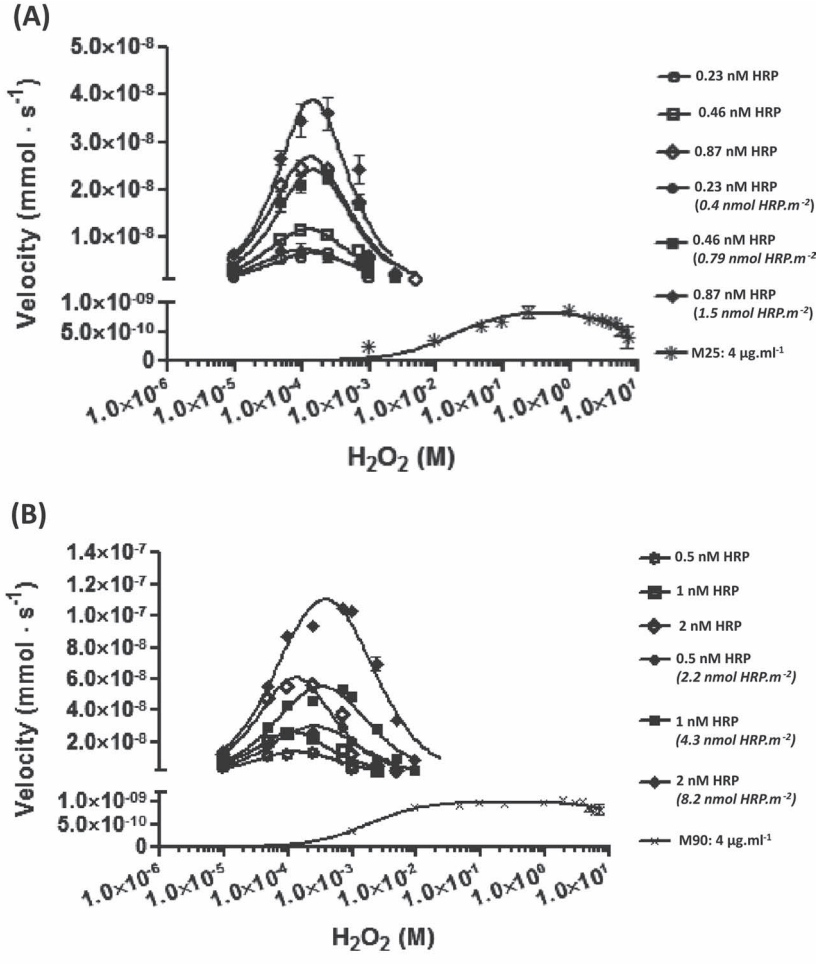

Figure 4. A–B) The effect of the H_2O_2 concentration on the initial reaction rates of the free HRP, and the M25- and M90-BNCs at 4 μg mL^{-1} of the bound fraction of enzyme (2.9×10^{-3} M malonate buffer, pH 3 at 25 °C): M25-BNC: 0.23×10^{-9} M HRP(•), 0.47×10^{-9} M HRP (■) and 0.87×10^{-9} M HRP (♦) (A); M90-BNC: 0.5×10^{-9} M HRP (•), 1×10^{-9} M HRP (■) and 2×10^{-9} M HRP M90-BNC(♦) (B). Free enzymes at corresponding concentrations: (○), (□), and (◊). The peroxidase-like activities of the magnetite MNPs at 4 μg mL^{-1} for the M25 and M90 (×) are shown for comparison.

increased velocity. Since the amount of bound enzyme differed between the M25- and M90-BNCs, Langmuir binding isotherms were used to calculate the fraction of HRP in solution and extract the kinetic parameters for the bound fraction of the enzyme only.

2.4. Velocities and Kinetic Parameters of the BNCs, HRP and the MNPs

In the following analysis, only the activity and kinetic parameters of the bound enzyme were used to assess the performance of the BNCs. For the M90-BNC, an enzyme-to-surface area ratio of 2.2–0.16 nmol m^{-2} resulted in total binding of the HRP. In contrast, for the M25-BNC, only 45% of the enzyme molecules were bound in the range of 40.0–1.5 nmol m^{-2} (Table 1). The initial reaction velocities for different H_2O_2 and HRP concentrations are presented in Figure 4. Peak velocities for the MNPs required molar concentrations of H_2O_2, whereas the HRP and BNC peak velocities were observed in the millimolar range for the peroxide. However, the M90-BNC peak velocities occurred at higher H_2O_2 concentrations than for both the M25-BNC and the free HRP (Figure 4B). The increased activity in comparison with the free enzyme was a function of H_2O_2 concentration (Figure S3, Supporting Information). This increased activity can be due to a higher BNC activity, a lower activity of the free enzymes due to higher substrate inhibition at the H_2O_2 concentrations used for comparison, or both (Figure 3A).

The initial reaction velocities and Equation 2 were used to estimate V_{max}, k_{cat}, K_i and K_m (**Figure 5**B–E). The V_{max} of the M25 or M90 MNPs was several orders of magnitude lower than those of the free HRP and the BNCs. The turnover rates, k_{cat}, were very consistent within the free-HRP and the M25- and M90-BNC datasets (Table S2, Supporting Information). The K_m values for the MNPs confirmed that a relatively high H_2O_2 concentration was required for the MNPs to exhibit any peroxidase-like activity, and their peroxidase-like activities were not substrate-inhibited, as shown by their high K_i values. The range of H_2O_2 concentrations required for the MNPs to show significant peroxidase-like activity was at least two orders of

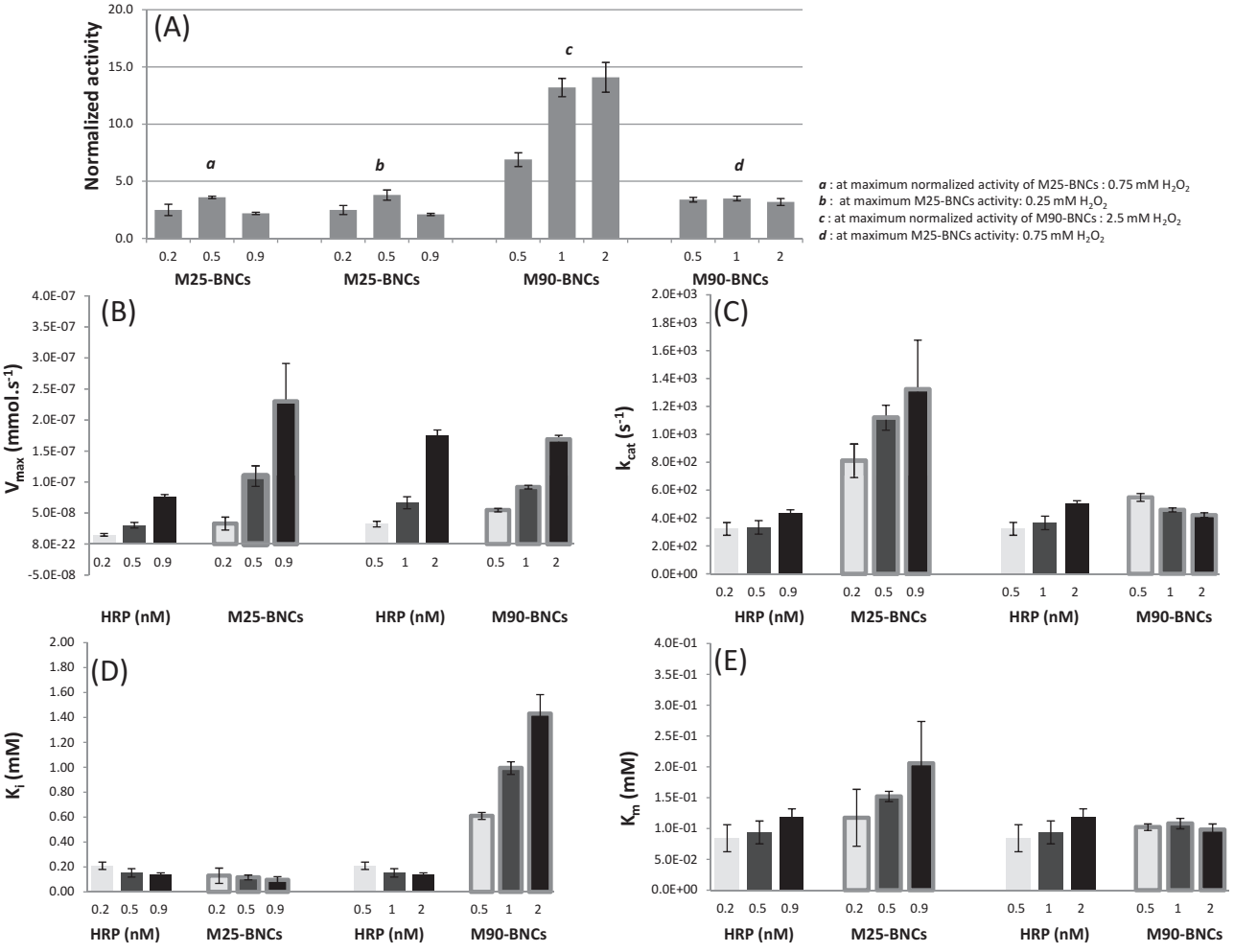

Figure 5. A) Normalized activities of the M25- and M90-BNCs. B–E), V_{max} (B), k_{cat} (C), K_i (D) and K_m (E) of HRP, the M90-BNC and the M25-BNC (□) at 4 μg mL^{-1} magnetite and 0.5×10^{-9}, 1×10^{-9} and 2×10^{-9} M total HRP, corresponding to 2.54, 4.95 and 9.43% Q_m for M25-BNC and 17.86, 30.30 and 46.51% Q_m for M90-BNC. The values on the *x* -axis show the concentration of the bound enzyme.

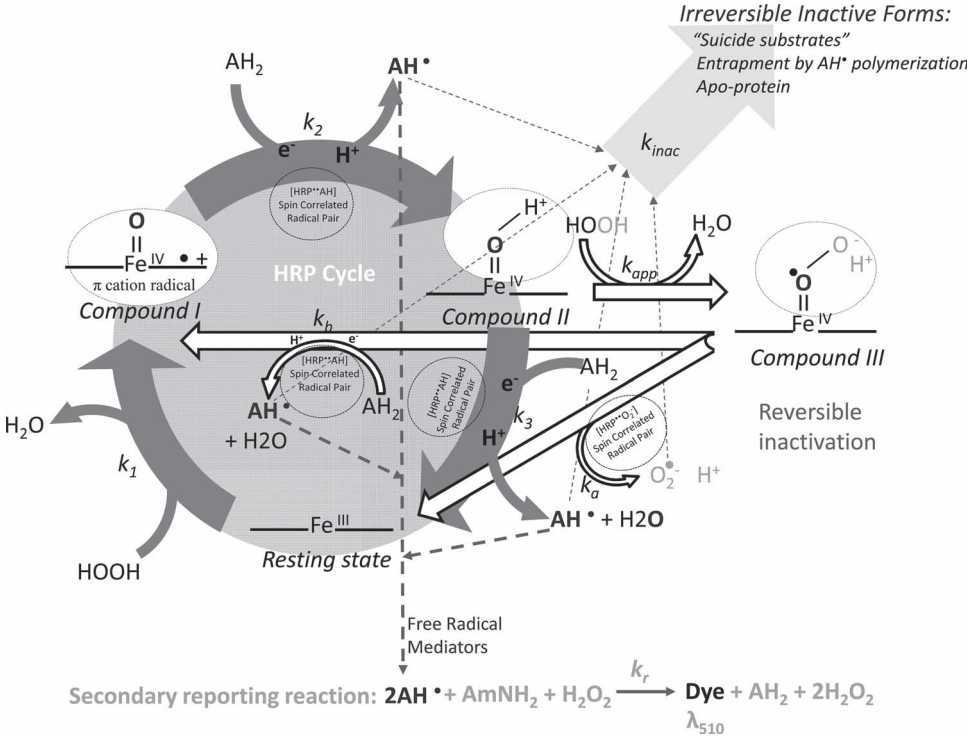

Figure 6. Detailed diagram of the HRP cycle and reactions in the H_2O_2/phenol/AAP assay used in this study. Grey arrows: non-inhibited cycle; hollow arrows: reversible inhibition via Compound III formation in excess H_2O_2; light-grey arrow: irreversible inhibition at high concentration of free radicals; dashed circles: reaction steps potentially susceptible to magnetic-field effects. Rate constants from the literature are provided (Table S3, Supporting Information).

magnitude higher than those typical in HRP-mediated reactions. The efficiencies of the M25 and M90 MNPs, as estimated by $k_{cat}[MNP]/K_m$ were 56 and 1130 s^{-1} M^{-1}, respectively. In comparison, the efficiency of the free HRP was 3.9×10^6 s^{-1} M^{-1}. The normalized comparison of the turnover of the reaction per accessible Fe atom ($k_{cat[Fe]}$ (Table S2, Supporting Information)) showed that the coordinated Fe atom in HRP was at least seven orders of magnitude more effective than any atom of Fe at the surface of an MNP. Although the nanoparticles did exhibit peroxidase-like activities at high H_2O_2 concentrations, the increase in overall peroxidase activity was, therefore, not due to any intrinsic peroxidase-like activity from the MNPs alone in the range of H_2O_2 concentrations that is compatible with optimal HRP activities.

2.5. M25-BNC versus M90-BNC: Fastest Turnover versus Lower Inhibition

The BNCs formed with M25 had the highest K_m (Figure 5C). The M25-BNC had V_{max} and k_{cat} two to three times greater than the free enzyme at the same concentration. Also, the k_{cat} of the M25-BNCs increased with the fraction of bound enzyme, while the K_i was in the same range as that of the free HRP. At 0.5×10^{-9} M of bound enzyme, the efficiencies of the MNPs as estimated by k_{cat}/K_m were 6.75×10^6 and 5.5×10^6 s^{-1} M^{-1} for the M25-BNCs and the M90-BNCs, respectively. These kinetics results are consistent with the trends observed with the reaction velocities (Figure 4). The M90-BNC had a K_i about 10 times greater than that of the free HRP, while its V_{max} was similar (Figure 5B). The higher K_i for M90 (Figure 5D) indicates a lower extent of substrate inhibition from H_2O_2 compared with the free enzyme and the M25-BNCs. The increase of the normalized activity in the case of the M90-BNC was more likely to be the result of lower substrate inhibition. A rather simple explanation is that the M90 aggregates limited the rate of diffusion of H_2O_2 to the enzymes trapped in the mesoporous MNP clusters. The apparent concentration of substrate in the bulk solution would be higher than its real concentration in the immediate vicinity of the enzymes, protecting them, de facto, from substrate-inhibition by limiting the accumulation of the poorly reactive Compound III (**Figure 6**). Excess H_2O_2 primarily inhibits the HRP reaction cycle by favoring the formation of Compound III, for which the rates of formation are faster than the reverse reaction rates by one to two order of magnitude (Table S3, Supporting Information). Other mechanisms can irreversibly inactivate the HRP, including high concentrations of free-radicals that can react with each other or with the enzyme itself. However, in the present system, the free-radicals readily reacted with the dye precursor (AAP) limiting the accumulation of free-radicals to irreversible inhibitory levels; thus, HRP inhibition was mostly H_2O_2-driven and, overall, reversible within the duration of the experiments. Lower inhibition would then be a direct effect of the local H_2O_2 concentration at the nanoscale. Although a diffusion-limited mechanism appeared to control the activity of the M90-BNC, the increased activity

of the enzymes at the local scale by an ISC mechanism is also probable. Finally, a magnetic-field effect on Compound III reversion rates[25,33,34] cannot be ruled out either, as both reactions involve radical pairs either by returning Compound III to the resting state via the superoxide ion or to Compound I via free-radical production (Figure 6).

The M90-BNC activities were further investigated with different buffers, pH and temperature (**Figure 7**). A similar increase of the M90-BNC activity was observed in inorganic and organic buffers and across the range of temperature tested. The BNCs were more efficient at lower temperatures than the HRP alone, as the free enzyme had higher velocities at higher temperatures. The M90-BNCs were pH sensitive, with the velocities increasing with pH, while the normalized activity was pH dependent in inorganic buffers. No effect due to pH was observed with organic acid buffers.

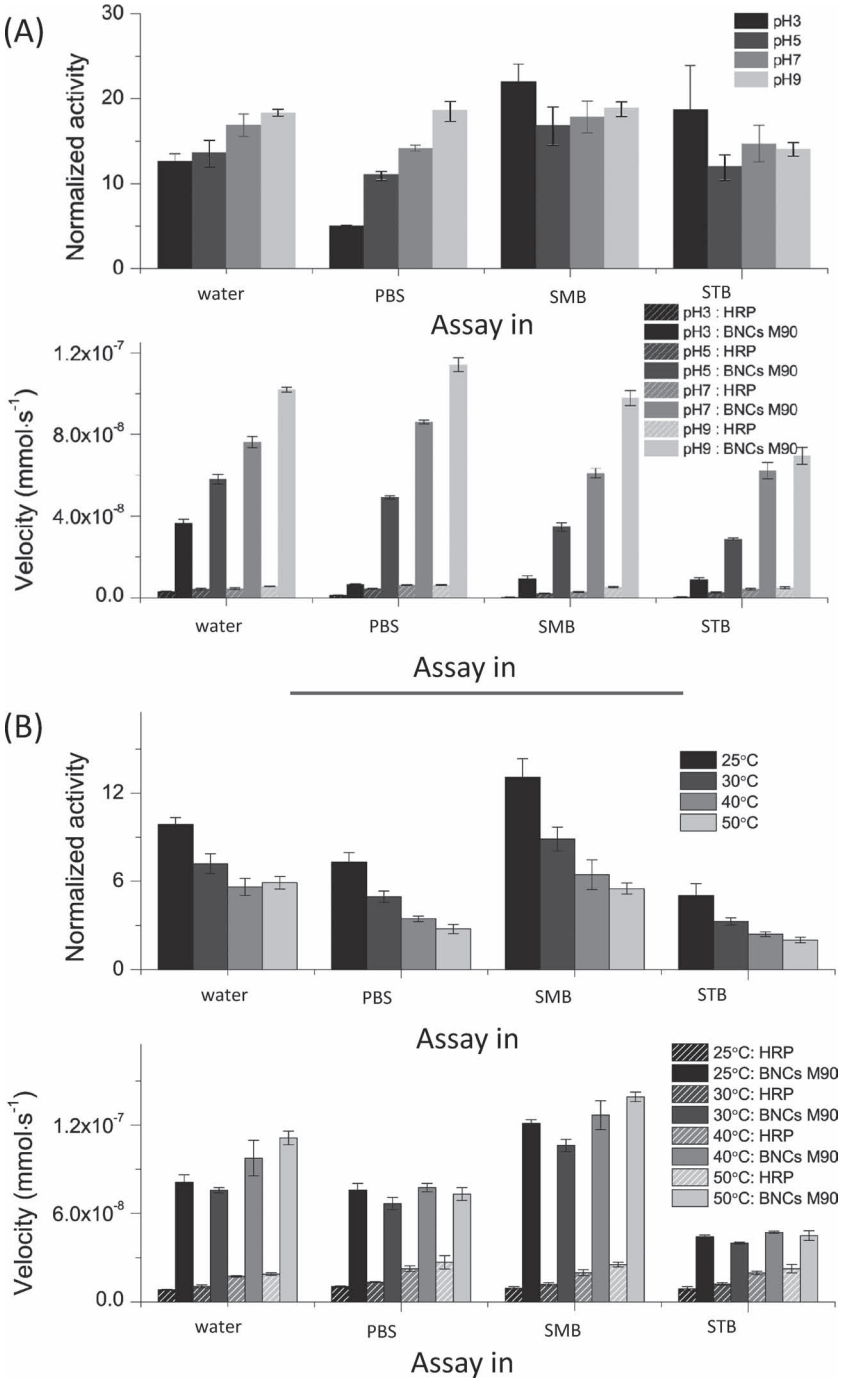

Figure 7. A,B) Effects of pH at $T = 25$ °C (A) and temperature at pH = 3 (B) on the activity of HRP in phosphate buffered saline (PBS), sodium malonate (SMB) and sodium tartrate (STB) buffers at 1×10^{-9} M and M90-BNCs (1×10^{-9} M HRP, 5×10^{-3} M H_2O_2, 4 μg mL^{-1} M90, 100% HRP adsorbed, 30.3% Q_m).

3. Discussion

3.1. Mesoporosity and Magnetic Field Effects at the Nanoscale (nano-MFE)

The potential of exploiting the magnetic field effect of magnetite MNPs in combination with a peroxidase enzyme is demonstrated and it was shown to modify the kinetics of the peroxidase activity of enzyme-nanoparticles complexes. An enhanced activity, compared with the free enzyme, was observed at different pHs, temperatures and buffers for all of the BNCs tested. In all of the cases, the observed properties were the result of the HRP-MNP complex (Figure S7, Supporting Information) and were not due to the MNPs themselves. The increased turnover of free-radical production is evidence of a magnetic field effect (MFE) arising from the MNPs at the nanoscale. The M90-BNC also exhibited lower sensitivity towards H_2O_2 inhibition, which could be related to the mesoporous ultrastructure of the aggregates and the distribution of the enzyme within the clusters.

The MFE-related enhanced activity of the peroxidase could arise from a diversity of fundamental mechanisms controlling the interactions between the enzyme and MNPs and, particularly, the rates of free-radical-pair recombination via intersystem crossing. ISC can be affected by magnetic fields in chemical reactions involving radical pairs via different mechanisms, depending upon the intensity of the magnetic fluxes. ISC appears to play a major role in the case of the M25-BNC, as shown by the large increase in velocity and the turnover of the reaction, as represented by the value of V_{max} being three times higher for the M25-BNC. The surface magnetic fluxes induced by both the primary M25 and M90 MNPs, and clusters thereof, were far stronger than the reported effective field necessary for ISC-mediated MFEs. For comparison, the effective hyperfine interaction field was reported to be

around 20 G in external-field experiments for similar free-radical species.[3,35] However, a striking difference with external field studies is that the heterogeneity and distribution of the nanoparticles also translate in the heterogeneity of the magnetic fields at the nanoscale. These results are consistent with the magnetic field effect theory, although the heterogeneous effects of local dynamic fields might play a major role in the overall ISC rate. The intensity of the magnetic field is a function of the size and distance to the surface of the nanoparticles or clusters. It has been hypothesized that even small variations of the magnetic field will result in drastic changes in enzyme activity.[35] The heterogeneity in the MNP size, although limited, might actually mask several local effective magnetic fields because of large variations in the magnetic-flux density. The ISC mechanism was calculated to be significant for superparamagnetic nanoparticles up to 30 nm in diameter and extend for several hundreds of nanometers from the MNP surface.[13] Considering the MNPs as magnetic elementary units, the range of magnetic-field intensity varied from about 700 G to 10 G within 100 nm from the nanoparticle surface (Figure S1, Supporting Information). Entrapped HRP molecules would not be further than 1.75 nm from the surface of the MNPs in the case of the M25-BNC (average pore size of 3.5 nm), and no less than 7.8 nm for the M90-BNC (average pore size of 15.6 nm), resulting in actual effective magnetic flux intensities ranging from 700 to 100 G for both the M25- and M90-BNCs. However, pinpointing the specific steps of the HRP catalytic cycle that are influenced by MNP-generated MFEs is made challenging by local magnetic flux effects.

3.2. Increasing the Potential and Application of Free Radical Producing Enzymes

Often, enzyme immobilization results in the alteration of native structures.[36,37] Thus, immobilization by adsorption, complexation or covalent linking is often accompanied with a loss of catalytic activity. In contrast, the BNCs showed increased activities (Video 1, Supporting Information) and, in addition, they can be readily recovered and reused[38,39] as catalysts (Figure S7, Video 2, Supporting Information). Entrapped peroxidase enzymes within mesoporous clusters of MNPs presenting MFE-doping of activity offer powerful alternatives to exploit enzymatic free radical driven biochemical reactions, including biosensors with increased sensitivity and resilience,[20,40] bleaching bioprocesses[41] and industrial catalysts for polymerizations reactions and decontamination of aromatic contaminants in water.[42,43] The aggregate morphology, the local field's intensity within the clusters, the pore structure and the diffusion properties contribute to a complex heterogeneous reaction; further studies to elucidate the influence of these various parameters on peroxidase reaction schemes are likely to benefit the development of BNCs. BNCs formed with peroxidases, or potentially other magnetosensitive enzymes, would broadly benefit a range of new and efficient bioprocesses for green chemistry applications.[44]

4. Conclusions

Our results demonstrate the potential of increasing the versatility of free radical producing enzymes using MNP-generated MFEs at the nanoscale, while exploiting the cluster properties of these self-assembled nanostructures. A magnetic-field effect at the nanoscale (nano-MFE) is responsible for an increased turnover of the enzymes associated with the MNPs, or in close vicinity of their surface. In addition, the mesoporous structure of the clusters can be responsible for the lower inhibition of the peroxidase due to diffusion limitations of the substrates at inhibitory levels. This work illustrates the importance of simultaneously exploring, and precisely understanding, the biochemistry of relevant biomolecules, while controlling key parameters of their local environment at the nanoscale. In the case of HRP, the local nano-MFE and the mesoporous nature of the MNP clusters appear to both act in concert to tune the biochemistry, and thus the overall kinetics and activities of the enzyme. Because of their magnetic nature, the resulting hybrids can be readily recovered and reused, and because of the low concentration of peroxide requirements, functionalized assemblies of MNPs with peroxidases are more interesting materials as biocompatible catalysts than MNPs alone. A precise understanding of the finely regulated reaction schemes of peroxidase enzymes is necessary to elucidate the observed increased activities of enzyme-MNPs associations compared with the free enzyme and to tailor and engineer new families of biocatalysts with improved efficiencies for new bioprocesses. Self-assembled MNP structures with embedded biocatalysts should be explored for other biological systems, in which reducing the energy levels of biochemical reactions by magnetic field effects at the nanoscale would be advantageous and/or for which the entrapped biomolecules would benefit from physical shielding and chemical protection against diffusible inhibitors.

5. Experimental Section

Materials and Reagents: Horseradish peroxidase (HRP) (E.C. 1.11.1.7, type VI-A) was purchased from Sigma –Aldrich. Its Reinheitszahl index (OD A_{403}/A_{280}) was found to be around 2.9. Phenol and AAP were obtained from Sigma–Aldrich (98% purity). Phosphate buffered saline (PBS) (pH = 7.4 and 67×10^{-3} M) was purchased from Invitrogen. Hydrogen peroxide, $FeCl_3 \cdot 6H_2O$, and $FeCl_2 \cdot 4H_2O$ were obtained from Sigma –Aldrich and used without further purification. The malonate and tartrate disodium salts were obtained from Fluka.

Magnetite-Particle Synthesis and Characterization: The magnetite nanoparticles were synthesized by coprecipitation of Fe^{2+} and Fe^{3+} under alkaline conditions in a bubbling nitrogen atmosphere at 25 °C (M25) or 90 °C (M90). An acidic solution (25 mL) of the iron salts (2 g of $FeCl_2 \cdot 4H_2O$ and 5.2 g of $FeCl_3 \cdot 6H_2O$) was added dropwise to NaOH (250 mL, 1.5 M) under constant stirring. Non-oxidizing conditions were achieved by bubbling all of the solutions with nitrogen for 15 min prior to reaction. The instantaneous black precipitation of Fe_3O_4 was captured with a neodymium magnet, washed and neutralized, and kept in distilled water until further use.

X-ray-diffraction (XRD) patterns were acquired using a Scintag Inc. θ–θ diffractometer equipped with a germanium detector, using Cu K_α radiation. The lattice constants and crystallite sizes were evaluated using Jade software (Materials Data Incorporated, MDI, USA). The lattice constants were calculated from the first four peaks at low angles. The full width half-maximum (FWHM) values were used in the Scherrer equation[45] to calculate the crystallite sizes. The magnetic properties were measured using an MPMS XL (Quantum Design) magnetometer, utilizing superconducting quantum interference device (SQUID) technology. The magnetization hysteresis curves were determined at 300 K for external magnetic fields ranging from 40 Oe to 50 kOe.

TEM-image processing was used to measure the average particle size, size distribution and cluster sizes. TEM measurements were performed using an ultrahigh vacuum scanning TEM (UHV-STEM) instrument (VG, UK). The images were processed using Image Analysis Image J software (NIH, Washington DC) and JMicroVision (V1.27). Nanoparticle and cluster size distributions were calculated from a minimum of 1000 particles. Nitrogen adsorption-desorption isotherms were obtained using a Micrometrics ASAP 2020 physisorption instrument. Pore size distributions were calculated from the N_2 adsorption isotherm using the Barrett–Joyner–Halenda (BJH) method.

Quantification of Adsorbed HRP onto Nanoparticles by Quantitative High-Throughput Fourier Transform IR (QHT-FTIR) Spectroscopy: The adsorption of HRP onto magnetite nanoparticles in water was investigated by QHT-FTIR spectroscopy.[46,47] The concentration of the stock solutions was determined from the absorbance of the Soret heme signal at 403 nm ($\varepsilon = 1.02 \times 10^5$ M^{-1} cm^{-1}). Magnetite suspensions (250, 500, and 750 μg mL^{-1}) were sonicated for 10 min and mixed with HRP solutions ranging from 0.25–7.5 $\times 10^{-6}$ M. The mixtures were incubated on a shaker at 4 °C overnight to reach equilibrium. Free enzyme molecules were removed using ultracentrifugation columns (molecular weight cut-off (MWCO) = 100 000 Da, Sartorius, Germany). The BNCs were recovered, sequentially boiled, disrupted and finally sonicated for 5 min to denature the proteins.

Quantification of the denatured HRP with magnetite nanoparticles was carried out using a high-throughput FTIR spectrometer (HTS-XT-Vertex70, Bruker, Germany). 50 μl of BNC slurry was dried out on a transmittance silicon 96-well plate at 60 °C under vacuum for 1 h and left to dry under vacuum at room temperature overnight. Spectra were recorded between 4000 and 400 cm^{-1}, with 32 scans, and the background was recorded before each sample. The samples were analyzed in triplicate; on-plate standards of magnetite and magnetite plus HRP were used to measure the concentrations of the proteins and nanoparticles in each sample (Figure S4, Supporting Information). Adsorption isotherm parameters were extracted by fitting the quadratic form of the Langmuir equation using a least-squares fitting method, using Matlab (Natick, MA, USA):

$$Q = \frac{Q_m K_a C^*}{1 + K_a C^*} \quad (1)$$

where Q is the adsorbed enzyme on the surface (nmol m^{-2}), C^* is the initial enzyme concentration (nmol m^{-2}), Q_m is the maximum amount of bound enzyme (nmol m^{-2}), and K_a is the adsorption constant (m^2 mol^{-1}). These parameters were applied in the kinetic experiments to calculate the bound fraction of HRP at equilibrium directly from the initial concentration of HRP.

HRP Kinetics and Parameter Estimation: The peroxidase activities of the native HRP and the BNCs were monitored using the chromogenic phenol/AAP assay, which generates phenoxy radicals that readily react with aminopyrene to form the pink-colored quinoneimine dye. An automated plate-reader (Synergy 4, Biotek) with injection capabilities and a temperature-controlled chamber was used to record the absorbance of the solution at 510 nm in 96-well plates (4 replicates) for 30 min. The standard reagent concentrations of the assay (200 μl) were 80 $\times$ 10^{-3} M and 13 $\times$ 10^{-3} M for the phenol and AAP respectively. Hydrogen peroxide was injected to initiate the reaction, with concentrations ranging between 10^{-7} M and 1 M. The background contribution due to the nanoparticles and substrates was subtracted. The quantity of free enzyme was calculated from the difference with the bound amount of enzyme estimated from the Langmuir adsorption model, as the quantity of free enzyme could not be estimated directly because of the low HRP concentrations and the high background from the MNPs. For each run, a velocity standard curve was established for the free enzyme (Figure S4, Supporting Information) and used to correct for the contribution of the free enzyme to the total activity when not all enzyme molecules were bound. The velocities (V) were calculated based on the initial rates of the reaction (Figure S5, Supporting Information). The specific activity, A (mmol$_{product}$ s^{-1} mmol$_{HRP}^{-1}$), was calculated as the ratio V/mmol$_{HRP}$ using an extinction coefficient of 6.58 $\times$ 10^3 M^{-1} cm^{-1} at 510 nm for the formation of quinoneimine dye.

A H_2O_2 substrate-inhibition model derived from the ping-pong bi-bi 2 substrate-inhibition model was used to extract the kinetic parameter of the reaction[48] by a least-squares fitting method using GraphPad Prism (La Jolla, CA, USA). The modified equation from the model is:

$$V = \frac{V_{max}[H_2O_2]}{K_m + [H_2O_2]\left(1 + \frac{[H_2O_2]}{K_i}\right)} \quad (2)$$

where V_{max} is the maximum enzyme velocity (mmol s^{-1}), the maximum rate the enzyme reaction can achieve, expressed in the same units as V, K_m is the Michaelis–Menten constant ($\times 10^{-3}$ M), and K_i is the inhibition constant for H_2O_2 ($\times 10^{-3}$ M). k_{cat} (s^{-1}) was calculated from V_{max} and the total quantity of bound HRP, Q (Equation 1), as a measure of the substrate turnover for the bound fraction of the enzyme for the estimated quantity of MNPs and for the Fe atoms in the heme or at the surface of the MNPs, assuming a density of 9.8 $\times$ 10^{18} Fe atoms per m^2.[49]

Supporting Information

Supporting Information is available from the Wiley Online Library or from the author.

Acknowledgements

P.K. gratefully acknowledges the support of a Thai government scholarship. This publication is based on work supported in part by Award No KUS-C1-018-02, made by King Abdullah University of Science and Technology (KAUST) and the US Department of Transportation under contract to the Northeast Sun Grant Initiative at Cornell University (US DOT Assistance # DTOS59-07-G-00052). This work made use of the Cornell Center for Materials Research Facilities supported by the National Science Foundation under Award Number DMR-0520404. The authors acknowledge the Nanobiotechnology Center (NBTC) and the Biofuels Research Laboratory (BRL) at Cornell University, Ithaca, NY, USA.

Received: October 6, 2011
Revised: November 18, 2011
Published online: February 15, 2012

[1] B. Rabinovitch, J. E. Maling, M. Weissbluth, *Biophys. J.* **1967**, *7*, 187.
[2] U. E. Steiner, T. Ulrich, *Chem. Rev.* **1989**, *89*, 521.
[3] C. Eichwald, J. Walleczek, *Biophys. J.* **1996**, *71*, 623.
[4] C. Eichwald, J. Walleczek, *Bioelectromagnetics* **1996**, *17*, 427.
[5] P. Gilch, F. Pollinger-Dammer, C. Musewald, M. E. Michel-Beyerle, U. E. Steiner, *Science* **1998**, *281*, 982.
[6] C. B. Grissom, *Chem. Rev.* **1995**, *95*, 3.
[7] M. Valentinuzzi, in *Biological effects of magnetic fields*, Vol. *1* (Ed: M. F. Barnothy), Plenum Press, New York **1964**, 63.
[8] A. C. Møller, L. F. Olsen, *J. Am. Chem. Soc.* **1999**, *121*, 6351.
[9] A. C. Møller, A. Lunding, L. F. Olsen, *Phys. Chem. Chem. Phys.* **2000**, *2*, 3443.
[10] E. Katz, O. Lioubashevski, I. Willner, *J. Am. Chem. Soc.* **2004**, *126*, 11088.
[11] V. K. Vanag, A. N. Kuznetsov, *Izv. Akad. Nauk SSSR, Ser. Biol.* **1988**, *2*, 215.
[12] S. Engström, in *Bioengineering and Biophysical Aspects of Electromagnetic Fields*, (Eds: F. S. Barnes, B. Greenebaum), CRC Press, Boca Raton, FL **2006**.
[13] A. E. Cohen, *J. Phys. Chem. A* **2009**, *113*, 11084.

[14] K. M. Salikhov, Y. N. Molin, R. Z. Sagdeev, A. L. Buchachenko, *Spin Polarization and Magnetic Effects in Radical Reactions*, Elsevier, Budapest, Hungary **1984**.
[15] B. Brocklehurst, *Chem. Soc. Rev.* **2002**, *31*, 301.
[16] M. S. T. Afanasyeva, M. B. Taraban, P. A. Purtov, T. V. Leshina, C. B. Grissom, *J. Am. Chem. Soc.* **2006**, *128*, 8651.
[17] L. Gao, J. Zhuang, L. Nie, J. Zhang, Y. Zhang, N. Gu, T. Wang, J. Feng, D. Yang, S. Perrett, X. Yan, *Nat. Nanotechnol.* **2007**, *2*, 577.
[18] F. Yu, Y. Huang, A. J. Cole, V. C. Yang, *Biomaterials* **2009**, *30*, 4716.
[19] N. G. Chalkias, P. Kahawong, E. P. Giannelis, *J. Am. Chem. Soc.* **2008**, *130*, 2910.
[20] A. M. Azevedo, V. C. Martins, D. M. F. Prazeres, V. Vojinović, J. M. S. Cabral, L. P. Fonseca, in *Biotechnology Annual Review*, Vol. 9, (Ed: M. Raafat El-Gewely) Elsevier, Amsterdam, The Netherlands **2003**, p. 199.
[21] N. C. Veitch, *Phytochemistry* **2004**, *65*, 249.
[22] M. B. Arnao, M. Acosta, J. A. del Rio, R. Varón, F. García-Cánovas, *Biochim. Biophys. Acta - Protein Struct. Mol. Enzymology* **1990**, *1041*, 43.
[23] K. J. Baynton, J. K. Bewtra, N. Biswas, K. E. Taylor, *Biochim. Biophys. Acta - Protein Struct. Mol. Enzymology* **1994**, *1206*, 272.
[24] O. M. Lardinois, M. M. Mestdagh, P. G. Rouxhet, *Biochim. Biophys. Acta - Protein Struct. Mol. Enzymology* **1996**, *1295*, 222.
[25] J. A. Nicell, H. Wright, *Enzyme Microbial Technol.* **1997**, *21*, 302.
[26] Q. Huang, Q. Huang, R. A. Pinto, K. Griebenow, R. Schweitzer-Stenner, W. J. Weber, *J. Am. Chem. Soc.* **2005**, *127*, 1431.
[27] M. B. Taraban, T. V. Leshina, M. A. Anderson, C. B. Grissom, *J. Am. Chem. Soc.* **1997**, *119*, 5768.
[28] A. R. Jones, N. S. Scrutton, J. R. Woodward, *J. Am. Chem. Soc.* **2006**, *128*, 8408.
[29] P. Roach, D. Farrar, C. C. Perry, *J. Am. Chem. Soc.* **2006**, *128*, 3939.
[30] L. Wang, Q. Zhou, T. Lu, X. Ding, X. Huang, *J. Biol. Inorg. Chem.* **2010**, *15*, 1063.
[31] D. Takahashi, Y. Kubota, K. Kokai, T. Izumi, M. Hirata, E. Kokufuta, *Langmuir* **2000**, *16*, 3133.
[32] W. Chouyyok, J. Panpranot, C. Thanachayanant, S. Prichanont, *J. Mol. Catal. B: Enzymatic* **2009**, *56*, 246.
[33] R. Carvalho, F. Lemos, M. Lemos, V. Vojinovi , L. Fonseca, J. Cabral, *Bioprocess Biosyst. Eng.* **2006**, *29*, 99.
[34] V. Vojinovic, R. H. Carvalho, F. Lemos, J. M. S. Cabral, L. P. Fonseca, B. S. Ferreira, *Biochem. Eng. J.* **2007**, *35*, 126.
[35] C. F. Eichwald, J. J. Walleczek, *J. Chem. Phys.* **1997**, *107*, 4943.
[36] W. N. a. T. Zoungrana, *Biotechnol. Appl. Biochem.* **1998**, *28*, 133.
[37] M. Lundqvist, I. Sethson, B.-H. Jonsson, *Langmuir* **2004**, *20*, 10639.
[38] F. Fang, J. Satulovsky, I. Szleifer, *Biophys. J.* **2005**, *89*, 1516.
[39] A. Sharma, Q. You, J. Antony, D. Meyer, P. Kornacki, A. Paszczynski, *IEEE Trans Magn.* **2007**, *43*, 2418.
[40] B. X. Gu, C. X. Xu, G. P. Zhu, S. Q. Liu, L. Y. Chen, M. L. Wang, J. J. Zhu, *J. Phys. Chem. B* **2009**, *113*, 6553.
[41] A. Bódalo, J. Bastida, M. Máximo, M. Montiel, M. Gómez, M. Murcia, *Bioprocess Biosyst. Eng.* **2008**, *31*, 587.
[42] K. Tatsumi, S. Wada, H. lchikawa, *Biotechnol. Bioeng.* **1996**, *51*, 126.
[43] W. Edwards, W. D. Leukes, J. J. Bezuidenhout, *Desalination* **2002**, *149*, 275.
[44] K. Sanderson, *Nature* **2011**, *469*, 18.
[45] B. D. Cullity, S. R. Stock, *Elements of X-Ray Diffraction*, Prentice-Hall Inc., Englewood Cliffs, NJ **2001**.
[46] Z. G. Peng, K. Hidajat, M. S. Uddin, *J. Colloid Interface Sci.* **2004**, *271*, 277.
[47] S. C. Corgie, H. M. Smith, L. P. Walker, *Biotechnol. Bioeng.* **2011**, *108*, 1509.
[48] Y.-J. Choi, H. J. Chae, E. Y. Kim, *J. Biosci. Bioeng.* **1999**, *88*, 368.
[49] K. Otto, M. Shelef, *J. Catal.* **1970**, *18*, 184.